

# Broadband Microwave Signal Processing Based on Photonic Dispersive Delay Lines

Jiejun Zhang, *Student Member, IEEE*, and Jianping Yao, *Fellow, IEEE*  
(Invited Paper)

**Abstract**—The development of communications technologies has led to an ever-increasing demand for a higher speed and wider bandwidth of microwave signal processors. To overcome the inherent electronic speed limitations, photonic techniques have been developed for processing of ultrabroadband microwave signals. A dispersive delay line (DDL) is a key photonic device that can be used to implement signal processing functions, such as time reversal, time delay, dispersion compensation, Fourier transformation, and pulse compression. Compared with an electrical delay line, a photonic DDL has a much wider bandwidth and can be used for processing a microwave signal with a much wider bandwidth. In this paper, we review our recent work using photonic DDLs for processing of broadband microwave signals. Two types of DDLs are to be discussed, a linearly chirped fiber Bragg grating-based DDL and an optical dispersive loop-based DDL. Signal processing functions including microwave time reversal, microwave temporal convolution, time-stretched sampling, microwave waveform generation with an extended temporal duration, and wideband true-time delay beamforming are discussed.

**Index Terms**—Dispersive delay line (DDL), linearly chirped fiber Bragg grating (LCFBG), microwave photonics, microwave signal processing, recirculating loop.

## I. INTRODUCTION

A DELAY line is one of the fundamental elements for analog signal processing. A delay line can be implemented electrically and optically. An electrical delay line can generate a time delay from a few nanoseconds to a few microseconds [1]. Different approaches have been proposed to realize an electrical delay line, such as a long electrical cable, a surface acoustic wave (SAW) device [2]–[7], an electromagnetic bandgap (EBG) element [8]–[10], and an integrated circuit (IC) [11]–[13]. The major limitations of using an electrical delay line for signal processing are the narrow operation bandwidth and small time delay. In general, a delay line with a large bandwidth and large time delay is required for wideband signal processing [14], [15].

There has been an increasing interest in using photonics to generate and process broadband microwave signals, thanks to the ultrawide bandwidth offered by photonics [16], [17]. A photonic delay line is a key element in a photonic

signal processor to generate a tunable time delay over a broad bandwidth. A photonic delay line can be implemented using a single-mode fiber (SMF), a dispersion compensating fiber (DCF), a fiber Bragg grating (FBG) [18], an integrated waveguide [19]–[22], or a photonic crystal waveguide [23], [24].

A photonic dispersive delay line (DDL) is a special delay line implemented in the optical domain that is able to introduce different time delays to different spectral components of a signal. Various signal processing functions implemented based on photonic DDLs have been demonstrated, which include microwave filtering [25]–[27], Fourier transformation [28]–[30], pulse compression [31], [32], frequency up-conversion [33], [34], temporal stretching [35]–[43], true-time delay beamforming [44], [45], and time reversal [46], [47]. So far, the implementation of such signal processing functions for practical applications is mainly limited by either the maximum dispersion or the bandwidth of the photonic DDLs, which would limit the temporal duration or the bandwidth of a microwave signal that can be processed by such a signal processor. An SMF- or DCF-based DDL usually has a small dispersion coefficient of hundreds of ps/nm. An FBG-based DDL with both large dispersion coefficient and bandwidth is difficult to fabricate.

In this paper, we review our recent work using photonic DDLs for processing of a microwave signal with simultaneously a large bandwidth and a long temporal duration. Two types of DDLs will be discussed: 1) a linearly chirped fiber Bragg grating (LCFBG)-based photonic DDL and 2) an optical dispersive loop (ODL)-based DDL. Signal processing functions including microwave time reversal [46], [47], microwave temporal convolution [48], time-stretched sampling [49], microwave waveform generation with an extended temporal duration [50], and wideband true-time delay beamforming [51], are discussed.

This paper is organized as follows. In Section II, the use of an LCFBG-based DDL for wideband microwave signal processing is discussed and two experimental demonstrations to implement microwave time reversal and microwave temporal convolution are provided. In Section III, the use of an ODL-based DDL with an ultralarge dispersion coefficient for wideband microwave signal processing is discussed and three experimental demonstrations to implement time-stretched sampling, waveform generation with an extended temporal duration and true-time delay beamforming are provided. In Section IV, the conclusion is drawn.

Manuscript received October 21, 2016; revised January 18, 2017; accepted January 23, 2017. Date of publication February 24, 2017; date of current version May 4, 2017. This work was supported by the Natural Sciences and Engineering Research Council of Canada.

The authors are with the Microwave Photonics Research Laboratory, School of Electrical Engineering and Computer Science, University of Ottawa, Ottawa, ON K1N 6N5, Canada (e-mail: jpyao@eecs.uottawa.ca).

Color versions of one or more of the figures in this paper are available online at <http://ieeexplore.ieee.org>.

Digital Object Identifier 10.1109/TMTT.2017.2665459

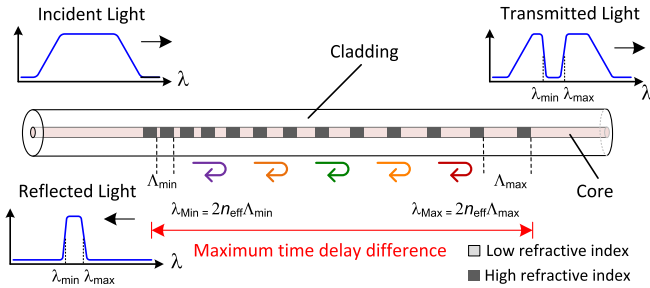


Fig. 1. Illustration for operation of an LCFBG. Blue: magnitude response of the LCFBG; Red: time delay response of the LCFBG.

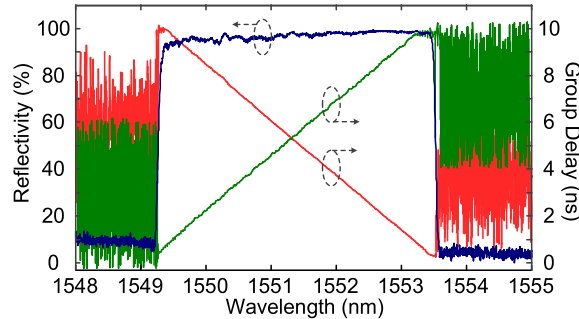


Fig. 2. Measured spectral response of an LCFBG [46], [47]. Blue: reflectivity. Red and green: the group delay response measured from the two different ends.

## II. LCFBG-BASED DDL FOR WIDEBAND MICROWAVE SIGNAL PROCESSING

An LCFBG is a fiber-optic component having a wide bandwidth and a linear group delay response within the bandwidth. The linear group delay or chromatic dispersion of an LCFBG is achieved by modulating the refractive index of the core of an optical fiber with a linearly increasing or decreasing pitch profile. An illustration of the operation of an LCFBG is shown in Fig. 1. As can be seen, the refractive index of the fiber core is altered with an increasing pitch profile from  $\Lambda_{\min}$  to  $\Lambda_{\max}$ , which can be done by UV illumination. As the reflection wavelength of an FBG is determined by the local grating pitch by  $\lambda = 2n_{\text{eff}}\Lambda$ , where  $n_{\text{eff}}$  is the effective refractive index of the optical fiber, a wavelength-dependent time delay corresponding to a different location where the light carrying a microwave signal is reflected is achieved. The maximum time delay difference  $\Delta\tau_{\text{max}}$  is determined by the physical length of the LCFBG, and the bandwidth is determined by the difference between the maximum and minimum grating periods. An LCFBG can be designed to have a large bandwidth up to a few THz and a large dispersion coefficient [18]. Fig. 2 shows an experimentally measured spectral response of a 1 m long LCFBG with a bandwidth of 4 nm and a central wavelength of 1551.4 nm. The dispersion coefficient of the LCFBG is measured to be  $\pm 2500$  ps/nm, with the sign determined by the end from which the group delay response of the LCFBG is measured. The maximum wavelength-dependent time delay difference is 10 ns, which is fundamentally limited by the 1 m long physical length of the LCFBG.

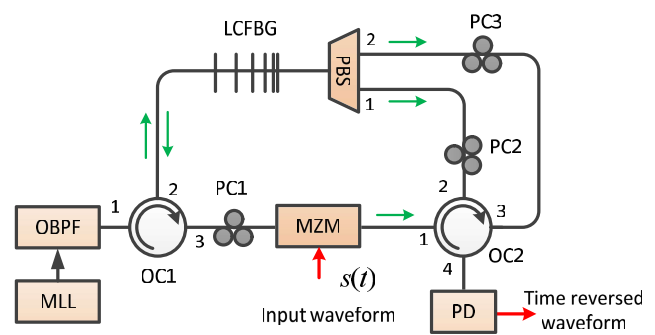


Fig. 3. Schematic of a microwave photonic signal processor for microwave time reversal [46], [47].

As a photonic DDL, an LCFBG can have a smaller loss and a greater compactness compared with other photonic dispersive devices such as an SMF and a DCF. For example, the dispersion coefficient of the LCFBG shown in Fig. 2 is equal to that of a 147 km long standard SMF. Thanks to the above advantages, LCFBG-based DDLs have been widely used for wideband microwave signal processing. In the following, we will review two solutions using an LCFBG-based DDL to perform wideband microwave time reversal and temporal convolution of microwave signals.

### A. Wideband Microwave Time Reversal

Microwave time reversal is a signal processing function to temporally reverse a microwave signal. It can find wide applications such as in a microwave imaging system to improve the resolution [52], [53], in a microwave communications system to mitigate the multipath problem and increase the power efficiency [54]–[57], and in a medical instrument for cancer detection [58], [59] and hyperthermia treatment [60]–[62].

Fig. 3 shows a microwave photonic signal processor to perform microwave time reversal based on an LCFBG-based DDL [46], [47]. A transform-limited optical pulse generated by a mode-locked laser (MLL) is filtered by an optical bandpass filter (OBPF) and sent to the LCFBG from its long wavelength end via a 3-port optical circulator (OC1). The optical pulse is then temporally stretched by the LCFBG. The LCFBG has a reflectivity of over 95% and a bandwidth of 4 nm, which is equal to that of the OBPF. Hence, the majority of energy of the optical pulse from the OBPF is reflected by the LCFBG and the transmitted energy is small and negligible. At the third port of OC1, a Mach-Zehnder modulator (MZM) is connected, to which a microwave waveform to be temporally reversed is applied. A polarization controller (PC1) is incorporated between OC1 and the MZM to align the polarization state of the optical pulse to the principal axis of the MZM, to minimize the polarization-dependent loss. At the output of the MZM, the optical pulse is directed into a 4-port OC (OC2). A polarization beam splitter (PBS) is used to connect the short wavelength end of the LCFBG to the second and third ports of OC2. Two additional PCs (PC2 and PC3) are employed between the PBS and OC2 to make sure that the light waves can be efficiently coupled to the LCFBG. The optical pulse injected to the first port of OC2 is directed to the second port, and then

sent to the short wavelength end of the LCFBG through the PBS. The optical pulse is then dispersed by the LCFBG and returned to the PBS. Since there is no Faraday effect involved in this process, the return light should have the polarization that perfectly matches the polarization of the lower arm of the PBS. Hence, the pulse is completely reflected to the second port of OC2. At the third port of OC2, an identical process occurs and the pulse is dispersed again by the LCFBG, but entering the LCFBG from the short wavelength end. The joint operation of OC2 and the PBS allows the optical pulse from the MZM to be independently and temporally dispersed by the LCFBG twice. The optical pulse is finally detected at a photodetector (PD) connected to the fourth port of OC2 and a time reversed microwave waveform is obtained at the output of the PD.

The time reversal is implemented relying on the complementary dispersion coefficients when an LCFBG is used twice by reflecting an optical signal from the two different ports. If an optical signal is entering the LCFBG from the left side, the corresponding impulse response is given by  $\exp[jt^2/(2\Phi)]$ , where  $\Phi$  is the dispersion coefficient of the LCFBG. Similarly, when the LCFBG is reflecting an optical signal from the right side, the dispersion coefficient and the impulse response of the LCFBG should be  $-\Phi$  and  $\exp[jt^2/(-2\Phi)]$ , respectively. When an electrical signal  $s(t)$  is applied to the MZM, the photocurrent at the output of the PD is given as

$$I(t) \propto G^2(\omega)s^2(-t)|_{\omega=-\frac{1}{\Phi}} \quad (1)$$

where  $G(\omega)$  is the optical spectrum of a pulse generated by the MLL and  $\omega$  is the optical angular frequency. Here,  $G(\omega)$  can be considered as unity since the optical pulse from the MLL is ultrashort, and its spectrum is ultrawide and flat. It can be seen from (1) that a temporally reversed signal of  $s(t)$  is achieved at the output of the PD. The squares in (1) are due to the intensity detection of the PD and can be calibrated.

The microwave time reversal system shown in Fig. 3 was experimentally evaluated using an LCFBG with a dispersion coefficient of  $\pm 2500$  ps/nm and a bandwidth of 4 nm. Fig. 4 shows the time reversal output when three different waveforms were used to test the operation of the system, which are a sawtooth waveform, a frequency-chirped waveform, and an arbitrary waveform. The similarity between the time reversed signal and the original signal is quantized by calculating the normalized root-mean-square deviation (NRMSD), which is the root-mean-square of the difference between the two signals normalized to the voltage range of the original signal. Note that the time-reversed signal is first flipped and then scaled to have the same voltage range with the original signal before the calculation of the NRMSD. The NRMSDs are calculated to be 7.01%, 8.08%, and 7.67% for the sawtooth waveform, the chirped waveform, and the arbitrary waveform, respectively, which confirm that the time reversed waveforms are in good agreement with the original waveforms. The maximum duration of the signals is 10 ns, which is determined by the maximum wavelength-dependent time delay provided by the LCFBG. The maximum bandwidth of the input signals is 4 GHz (the chirped waveform case), which is determined by the 10 Gb/s sampling rate of the electrical arbitrary waveform

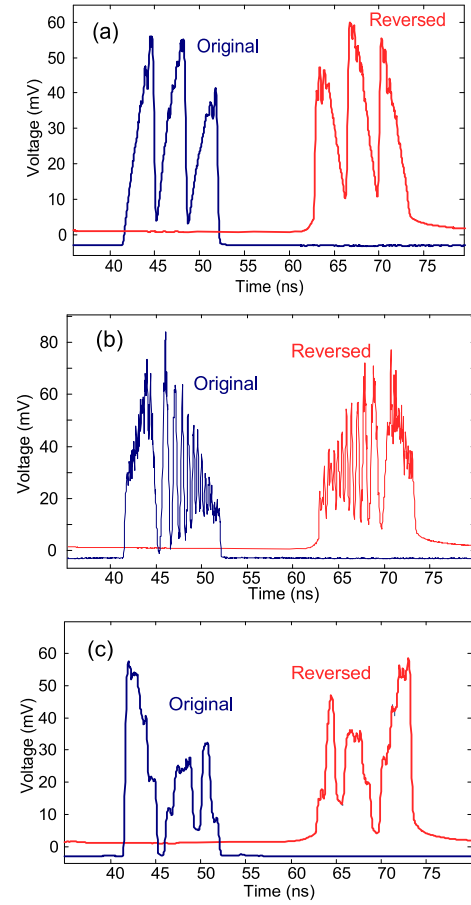


Fig. 4. Original and time reversed waveforms [46], [47]. (a) Sawtooth waveform. (b) Chirped waveform. (c) Arbitrary waveform.

generator (AWG) that is used to generate the test signals. The optical bandwidth of the time reversal system is limited by the bandwidth of the LCFBG. The LCFBG used for the experimental demonstration has a bandwidth of 4 nm, the optical bandwidth of the time reversal system is estimated to be 273 GHz.

Compared with the use of a digital circuit for the implementation of temporal reversal [54]–[62], a time reversal system based on photonics has a significantly wider operation bandwidth. In addition, temporal reversal using a digital circuit involves a complicated system composed of analog-to-digital conversion, digital signal processing (DSP), and digital-to-analog conversion. The use of a photonic solution would greatly simplify the implementation.

### B. Temporal Convolution of Microwave Signals

The temporal convolution between two signals of  $x(t)$  and  $y(t)$  is defined as

$$(x * y)(t) = \int_{-\infty}^{\infty} x(\tau)y(t - \tau)d\tau \quad (2)$$

where  $*$  denotes the convolution operation.

Temporal convolution between two signals is different from a filtering operation where a microwave signal is convolved with the impulse response of a microwave filter, which is

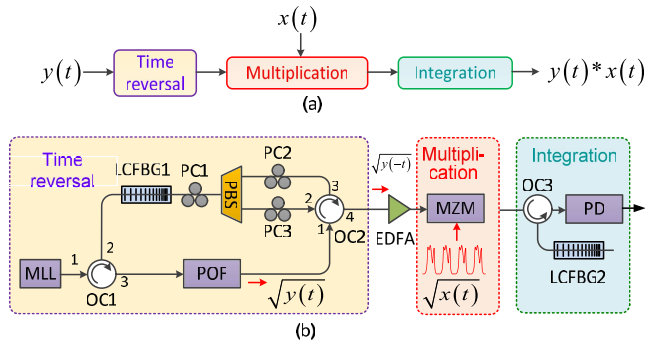


Fig. 5. (a) Illustration for the operation of a temporal convolution system [48]; (b) Schematic of the temporal convolution system composed of three subsystems.

not a time-domain signal. Some applications require that the two microwave signals to be convolved can be updated in real time [63], [64]. Temporal convolution can provide better flexibility in signal processing compared with a filtering operation since the spectral response of a microwave filter is fixed. So far, microwave convolution is performed by DSP techniques. The convolution of two microwave signals based on an analog system, especially a photonic analog system, has the potential to achieve a high operation bandwidth.

Fig. 5(a) shows a microwave temporal convolution system with two microwave signals of  $x(t)$  and  $y(t)$  to be convolved. The operation involves three operations, microwave time reversal, multiplication and integration [48], which are performed using three subsystems in the optical domain, as shown in Fig. 5(b). The first subsystem is to achieve time reversal, which is implemented based on the system shown in Fig. 3. An optical pulse in the pulse train generated by an MLL is first reflected by an LCFBG (LCFBG1) through an OC (OC1), and then spectrally shaped by a programmable optical filter (POF). The POF is configured to encode a microwave waveform to the optical carrier. The second subsystem is used to perform multiplication based on an MZM, to which a second microwave signal is applied via its electrical port. The integration is performed by a third subsystem that consists of a second LCFBG (LCFBG2) and a low-speed PD. Since the input signals are faster than the response time of the PD, the signal at the output of the PD is, in fact, proportional to the optical energy that it receives within its response time window, i.e., the integration of the power of the fast input signal. To get the integration for the amplitude of the signals indicated in (2), the input signals  $x(t)$  and  $y(t)$  should be preprocessed to have only positive values, and then converted to  $\sqrt{x(t)}$  and  $\sqrt{y(t)}$ . Note that if the integration is performed in the optical domain (without photo-detection), this preprocessing is not needed. In the following, for simplicity, we assume that the two input signals are given by  $\sqrt{x(t)}$  and  $\sqrt{y(t)}$ .

Different from the implementation of time reversal in Section II-A, here the POF is used to encode one of the microwave signals to the optical carrier to avoid the need of synchronization between the optical pulse from the MLL and the waveform  $\sqrt{y(t)}$  generated by the signal generator. The POF is configured to have a spectral response with a shape identical to that of the microwave signal,  $\sqrt{y(\omega)}$ , where  $\omega$  is

the optical angular frequency given by  $\omega = t/\Phi$  and  $\Phi$  is the dispersion coefficient of LCFBG1 when reflecting light from the left end. A time reversed signal  $\sqrt{y(-t)}$  will be generated at the output of the time reversal module, as discussed in Section II-A. Note that  $\sqrt{y(-t)}$  is repeating at a repetition rate identical to that of the pulse train from the MLL. An erbium-doped fiber amplifier (EDFA) is used after the time reversal subsystem to compensate for the losses of the POF, the PBS, and LCFBG1.

The optical pulse train in which an individual pulse is encoded by  $\sqrt{y(-t)}$  is then sent to the multiplication subsystem. The second microwave signal to be convolved,  $\sqrt{x(t)}$ , is generated by an AWG with a repetition rate slightly different from that of the pulse train from the MLL, and is applied to the MZM. The multiplied signal at the output of the MZM is then launched into LCFBG2 for integration. Note that LCFBG2 has a dispersion coefficient of 2500 ps/nm that is identical to that of LCFBG1 when reflecting an optical signal from the left end. The signal at the output of LCFBG2 is converted to the electrical domain at the PD. Integration will be performed at the same time thanks to the long response time of the PD.

Assume  $\sqrt{x(t)}$  and  $\sqrt{y(-t)}$  are generated with repetition periods of  $T_1$  and  $T_2$ , respectively. The two signals are then multiplied at the MZM. At LCFBG2, the multiplied pulse is compressed to have a temporal duration that is shorter than the response time of the PD. As a result, the PD measures the energy of each pulse in the pulse train, rather than the pulse shape. The photocurrent at the output of the PD for the  $n$ th multiplied pulse is given by

$$I'(n) = \Re \times \frac{1}{2\pi} \int_{\delta t} y(-t + nT_1)x(t - nT_2)dt. \quad (3)$$

It can be seen from (3) that a changing time delay difference of  $n \times (T_1 - T_2)$  is achieved between the replicas of  $x(t)$  and  $y(t)$  as  $n$  changes. Hence, the convolution result can be reconstructed from  $I'(n)$ . Note that  $I'(n)$  is the integration of the  $n$ th pulse in the pulse train. Therefore, it is discrete, and the corresponding unit time increase along the horizontal axis is  $|T_1 - T_2|$  for the convolution result.

Three waveform pairs are used to verify the operation of the temporal convolution system. First, two rectangular waveforms with an identical temporal width of 10 ns are used to evaluate the convolution operation. The two rectangular waveforms are generated by the POF and the AWG, and are shown in Fig. 6. Fig. 7 shows the experimentally obtained convolution output (blue line) and the ideal convolution result (red dotted line). The output signal is a series of short pulses, whose peak amplitude profile nicely fits with the ideal convolution. It should be noted that two timescales for the horizontal axes are used in Fig. 7, where the lower horizontal axis represents the time for the measured output and the upper horizontal axis represents the time for the convolution, which is recovered using  $n \times (T_2 - T_1)$  with  $n$  from 0 to  $N - 1$ . As we have discussed, the convolution results are discrete values given by the measured energies of the pulses. The corresponding time axis should also be discrete, with a unit time increment given by  $(T_2 - T_1)$ . In our case,  $(T_2 - T_1) = 0.01 \times T_1$ . The upper horizontal axis corresponding to the convolution is simply

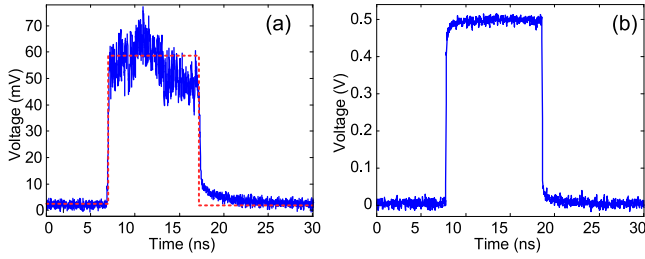


Fig. 6. Two rectangular waveforms used as two input waveforms for temporal convolution [48]. (a) Square root of  $y(t)$  encoded by the POF. Blue line: measured waveform at the output of the POF. Red dotted line: ideal rectangular waveform. (b) Square root of  $x(t)$  generated by the AWG.

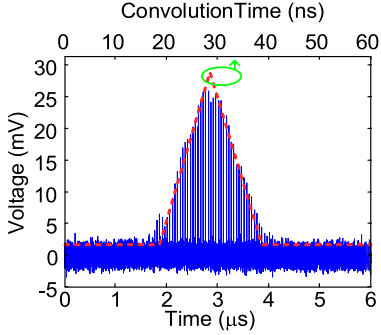


Fig. 7. Convolution between the two rectangular waveforms [48]. Red dotted line: theoretical convolution output of the two rectangular waveforms with the upper horizontal axis. Blue line: measured convolution output with the lower horizontal axis, which is a series of pulses with the peak amplitudes representing the convolution result.

obtained by multiplying the real time in the lower horizontal axis by 0.01.

Then, an asymmetric waveform which is an inverse sawtooth waveform is used to test the temporal convolution system. Again, by configuring the POF to have a spectral response of  $\sqrt{y(\omega)}$ , where  $y(\omega)$  has an inverse sawtooth shape, the square root of an inverse sawtooth waveform with a temporal duration of 10 ns is obtained at the output of the time reversal subsystem, as shown in Fig. 8(a). The waveform is then convolved with the rectangular waveform shown in Fig. 6(b). Fig. 8(b) shows the convolution result. A theoretically calculated convolution is also shown. As can be seen, good agreement between the theoretical and the measured results is achieved. For convolution operation, we know that  $x * y = y * x$ , i.e., no matter which function is temporally reversed, the convolution result should be the same. In our system, however, the convolution output may be temporally reversed if a different input signal is temporally reversed. But the sign of  $(T_2 - T_1)$  will also be different for  $x * y$  and  $y * x$ . The time in the horizontal axis for convolution  $n \times (T_2 - T_1)$  will then be reversed, which would result in consistent convolution results for both  $x * y$  and  $y * x$ .

Finally, we investigate the convolution between a complex waveform and a short pulse. The complex waveform is a three-cycle chirped waveform, which is generated by the AWG. The POF is configured to have a narrow passband of 20 GHz which leads to the generation of a short pulse with a temporal width of 400 ps after wavelength-to-time (WTT) mapping by LCFBG1. The generated square root of the three-cycle

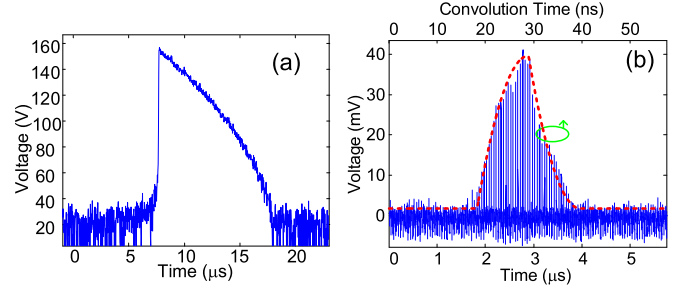


Fig. 8. (a) Square root of an inverse sawtooth waveform achieved at the output of the POF. (b) Convolution between a rectangular waveform and an inverse sawtooth waveform [48]. Red dotted line: theoretical convolution output of a rectangular waveform with an inverse sawtooth waveform. Blue line: measured convolution output of the system.

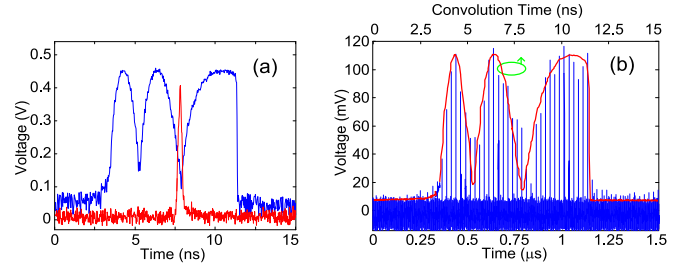


Fig. 9. (a) Square root of a short pulse achieved at the output of the POF (red) and square root of a three-cycle chirped waveform generated by the AWG (blue). (b) Convolution between a three-cycle chirped waveform and a short pulse. Red line: theoretic convolution result. Blue line: output of the convolution system, when the three-cycle chirped waveform is convolved with a short pulse with a temporal width of 400 ps [48].

chirped waveform and the short pulse are shown in Fig. 9(a). The convolution of a waveform and an ultrashort pulse (ideally a unit impulse function) should be the waveform itself. Fig. 9(b) shows the ideal convolution result and the measured convolution output of the system. Again, the measured result is in good agreement with theoretically calculated convolution result. For a complex waveform with more details, to get a more smooth convolution result, one may use a smaller value of  $|T_2 - T_1|$ , so that the convolution can be calculated with a higher time resolution, i.e., the input signals can have wider bandwidths.

### III. SIGNAL PROCESSING BASED ON AN ODL-BASED DDL

For microwave signal processing using a DDL, a large dispersion coefficient of the DDL is usually required. The dispersion coefficient of an LCFBG-based DDL is fundamentally limited by its physical length for a given bandwidth. Fabricating an LCFBG with a length longer than a few meters may not be practical. In addition, a long LCFBG is hard to package. Recently, we proposed a DDL with a large dispersion coefficient based on an ODL incorporating an LCFBG. An extremely large dispersion coefficient can be achieved by allowing an optical signal to recirculate in the loop for multiple round trips. For example, if an optical signal recirculates in an ODL for  $N$  round trips, the equivalent dispersion coefficient of the ODL-based DDL is  $N$  times that of the LCFBG.

In the following, we discuss the use of an ODL-based DDL to implement a time-stretched sampling system with a

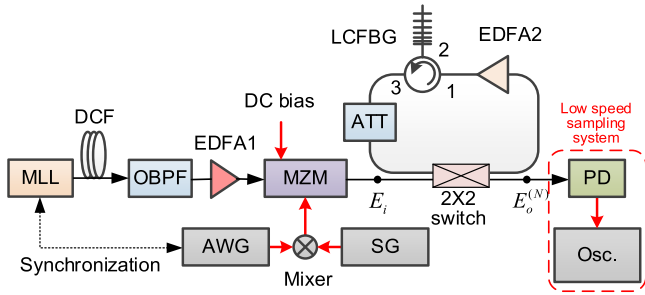


Fig. 10. Schematic of an optical time stretched sampling system [49]. Osc: oscilloscope.

large stretching factor [49], a photonic microwave waveform generator with an increased time duration [50], and a wideband photonic-assisted true-time delay beamforming network [51].

### A. Time Stretched Sampling

Time stretched sampling is a technique to sample a high speed signal using a low repetition rate sampling pulse train by temporally stretching the signal to be sampled, to slow down the signal. In an optical time-stretched sampling system, a microwave waveform to be sampled is modulated on a predispersed optical pulse, which, after being modulated by the microwave waveform, travels through a DDL a time-stretched microwave waveform is generated at the output of a PD [36]–[40], [43], [65]. To achieve temporal stretching with a large stretching factor, a DDL should have a large dispersion coefficient, in the order of several ns/nm, which is hard to achieve for a DDL based on an SMF, a DCF, or a single LCFBG.

An ODL-based DDL can be used to perform temporal stretch with a large stretching factor [49]. Fig. 10 shows an optical time-stretched sampling system using an ODL-based DDL. An optical pulse from an MLL is sent to a DCF with a dispersion coefficient of  $-339$  ps/nm where predispersion is realized. The predispersed optical pulse is then sent through an OBPF and an EDFA (EDFA1) to an MZM where a microwave waveform to be sampled is modulated on the predispersed optical pulse. The microwave waveform applied to the MZM is generated by mixing an electrical gate signal from an AWG with a sinusoidal microwave signal from a microwave generator (SG). The modulated signal is then sent to the ODL, in which an LCFBG with a dispersion coefficient of  $-1500$  ps/nm and a second EDFA (EDFA2) are incorporated. The modulated waveform is launched into the recirculating ODL through a  $2 \times 2$  optical switch. In the ODL, the LCFBG is used as a DDL and EDFA2 is used to compensate for the round-trip loss. An optical attenuator (ATT) is also included to provide a fine control of the loop gain. The time-stretched optical pulse at the output of the ODL is sent to a PD and sampled by a low-speed sampling circuit.

The frequency response of an LCFBG is

$$H_{\text{LCFBG}}(\omega) = \exp\left(-j\frac{\Phi}{2}\omega^2\right) \quad (4)$$

The frequency response of the ODL-based DDL considering an optical signal recirculating in the loop multiple times is

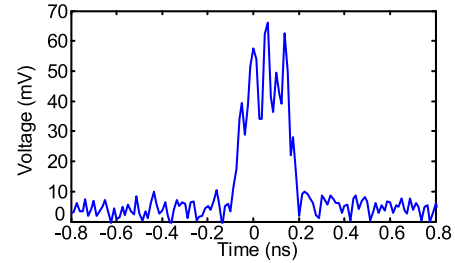


Fig. 11. Sampled waveform without passing through the ODL-based DDL [49].

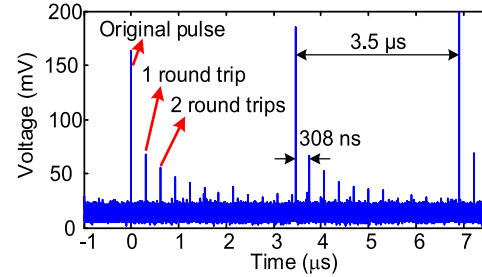


Fig. 12. Measured optical waveforms at the output of the ODL for different round trips [49].

given by

$$H_{\text{loop}}(\omega) = g^N \exp\left(-j\frac{N\Phi}{2}\omega^2\right) \quad (5)$$

where  $g$  is the net gain of the loop. By adjusting the pumping power to EDFA2 and the attenuation of the ATT,  $g$  can be tuned to be close to one. Then, the ODL-based DDL can be seen as a delay line with a dispersion coefficient of  $N\Phi$ . The stretching factor of the sampling system is given by

$$M = 1 + N\Phi/\Phi_D \quad (6)$$

where  $\Phi_D$  is the dispersion coefficient of the DCF. As  $N$  increases, the stretching factor is also increased.

The system is used to sample a 36 GHz sinusoidal signal with a time duration of 203 ps (corresponding to 7 sinusoidal cycles). The LCFBG has a dispersion coefficient of 1500 ps/nm. The detection is done using a PD with a bandwidth of 25 GHz and the sampling is done by an oscilloscope with a sampling rate of 80 Gs/s or a bandwidth of 32 GHz. The sampled signal without passing through the ODL-based DDL is shown in Fig. 11. For a 36 GHz signal, the temporal spacing between two sinusoidal cycles is 27.8 ps, which is smaller than the 40 ps response time of the PD, and is close to 12.5 ps sampling interval of the sampling system of 12.5 ps. The cycles of the sinusoidal signal cannot be identified by directly reconstructing the sinusoidal signal. In order to reconstruct the signal with the PD and the sampling system, time stretching should be used. The signal at the output of the ODL-based DDL after recirculating multiple times is shown in Fig. 12. To simplify the experiment, the  $2 \times 2$  optical switch was replaced by a  $2 \times 2$  optical coupler. Thus, the temporally stretched signal after each round trip is obtained at the output of the ODL, and a pulse burst with a decaying amplitude is seen. The decay

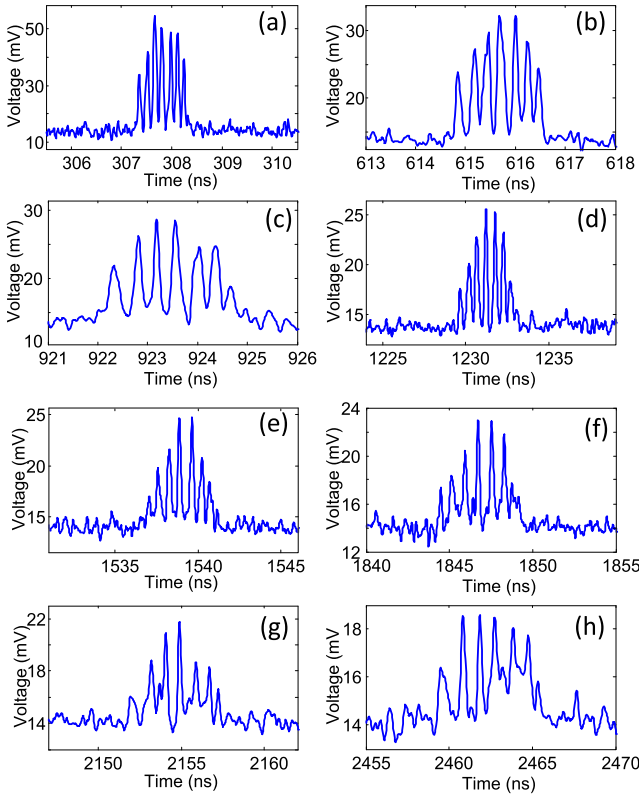


Fig. 13. Temporally stretched waveforms after different number of round trips [49]. (a) One round trip. (b) Two round trips. (c) Three round trips. (d) Four round trips. (e) Five round trips, (f) Six round trips. (g) Seven round trips. (h) Eight round trips. Note that the timescale is 1 ns/div in (a)–(c), and 5 ns/div in (d)–(h).

is due to the net loop gain, which is slightly smaller than one. The reason to keep the net gain smaller than one is to ensure that no lasing would occur in the loop. Zoom-in views of the waveforms after the pulse is stretched by the ODL-based DDL for 1–8 times are shown in Fig. 13(a)–(h). After one round trip, the pulse duration is stretched to around 1 ns and all the seven sinusoidal cycles with a temporal separation between two adjacent cycles of around 140 ps can be well constructed and identified, as shown in Fig. 13(a). The optical pulse is stretched with a stretching factor of around 5.

For the pulse after the eighth round trip, the equivalent dispersion coefficient is  $8 \times 1500 \text{ ps/nm} = 12000 \text{ ps/nm}$ . The measured waveform after the eighth round trip shows that the pulse duration is stretched to around 7 ns and the average temporal separation between two adjacent sinusoidal cycles is 1 ns. A stretching factor of 36 is obtained, which is close to the theoretically calculated stretching factor of 36.4. Assuming that the bandwidth of the system is limited by the oscilloscope used in our experiment, which is 32 GHz, the bandwidth of the sampling system can be as large as  $36 \times 32 = 1.15 \text{ THz}$ , corresponding to a time resolution of 347 fs. The maximum time duration of a microwave signal that can be sampled by the system in a single measurement is 203 ps. The time resolution and measurement duration of the system are comparable or better than other time stretched sampling systems reported in [35]–[43], but with a significantly reduced system complexity.

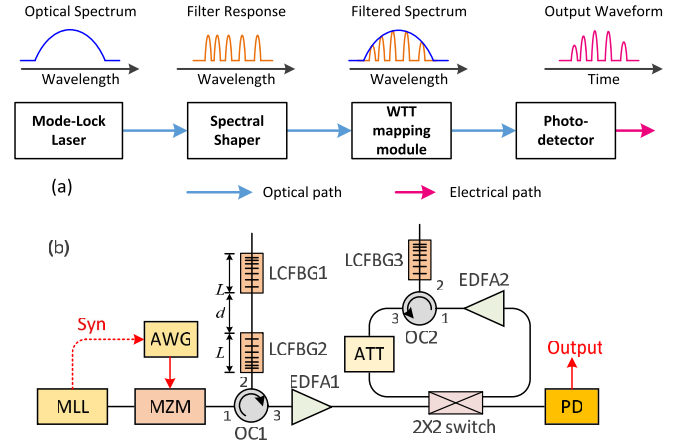


Fig. 14. (a) Waveform generation based on SS and WTT mapping in a DDL. (b) Schematic of a microwave waveform generator [50]. Syn: synchronization.

Thanks to the large dispersion coefficient of the ODL, the time stretched sampling system can achieve a larger stretching factor and a higher sampling rate with greater compactness compared with other systems in which only a DDL based on an SMF, a DCF, or a single-time used LCFBGs is employed [35]–[42]. In [43], a stretching factor of 250 is achieved by allowing the optical signal to propagate twice through a DCF with a length of 125 km by using a reflection mirror. Four Brillouin amplifiers are required to compensate for the propagation loss. However, the dispersion coefficient of the DCF is  $-10246 \text{ ps/nm}$ , which is still smaller than that of the ODL.

### B. Waveform Generation With an Extended Duration

A microwave waveform with a large time-bandwidth product (TBWP) can find numerous applications in microwave sensors [66], [67], spread-spectrum communications [68], microwave computed tomography [69], and modern instrumentation. An ODL-based DDL with a large dispersion coefficient can also be used for the generation of a microwave waveform with an extended time duration.

A microwave waveform can be generated based on spectral shaping (SS) and WTT mapping [65]. The operation of an SS-WTT mapping system is shown in Fig. 14(a). A spectral shaper is used to spectrally shape an ultrashort optical pulse from an MLL, to make the shaped spectrum to have a shape identical to the temporal waveform to be generated. A DDL is used to perform WTT mapping [50] to convert the spectrally shaped pulse, to a temporal pulse with a shape identical to the spectrum of the spectrally shaped pulse. To generate a microwave waveform with a longer time duration, a DDL with a larger dispersion coefficient may be used. Fig. 14(b) shows the schematic of a microwave waveform generator based on an SS-WTT mapping system in which the WTT mapping is done using an ODL-based DDL. An MLL is used to generate an ultrashort pulse train. To reduce the repetition rate, an AWG is used to generate a gate sequence to control the MZM to be on for one pulse and off for 16 pulses. Thus, the repetition rate is reduced by 17 times and the temporal spacing between

two adjacent pulses is increased by 17 times to give more temporal spacing for pulse stretching without causing overlap of adjacent pulses. The repetition-rate-reduced pulse train is then sent via an OC (OC1) to the spectral shaper which is a Fabry-Perot interferometer (FPI) formed by two LCFBGs with complementary dispersion (LCFBG1 and LCFBG2). Due to the wavelength dependent cavity length, a spectral response of the FPI with a free spectral range (FSR) that is linearly increasing or decreasing is produced. The FPI is then used to shape the spectrum of the ultrashort pulse from the MZM, so that a linearly chirped microwave waveform (LCMW) can be generated after WWT mapping performed by the DDL. To compensate for the loss caused by the MZM and the repetition rate reduction, an EDFA (EDFA1) is connected after the MZM. The spectrum-shaped pulse from the FPI is then sent to the ODL, in which a third LCFBG (LCFBG3) with a dispersion coefficient of 2500 ps/nm is incorporated via a second OC (OC2). A second EDFA (EDFA2) is employed in the ODL to provide an optical gain, and an ATT is incorporated to fine tune the attenuation, to make the net gain slightly less than 1 to avoid lasing. The temporally stretched pulse is then sent to a PD via a  $2 \times 2$  optical switch, and an LCMW with an extended temporal duration is obtained at the output of the PD.

The temporal duration of the generated waveform is given by

$$\Delta\tau = N\Phi_3\Delta\omega \quad (7)$$

where  $\Delta\omega$  is the spectral width of the optical pulse and  $N\Phi_3$  is the dispersion coefficient of the ODL-based DDL. The temporal duration of the generated microwave waveform can be significantly longer compared with the use of a DDL consisting of an LCFBG without an optical loop. The bandwidth of the generated waveform, on the other hand, is determined by both the dispersion coefficient of the ODL-based DDL and the LCFBGs that forms the spectral shaper, which is given by

$$\Delta f = \frac{4\Phi_1\Delta\omega}{\pi N\Phi_3} \quad (8)$$

where  $\Phi_1$  or  $-\Phi_1$  is the dispersion coefficient of LCFBG1 or LCFBG2 and  $\Phi_3$  is the dispersion coefficient of LCFBG3. The TBWP of the microwave waveform is expressed as  $TBWP = 4\Phi_1\Delta\omega^2/\pi$ , which is a constant, and is independent of  $N$ , i.e., the use of the ODL-based delay line does not increase the TBWP of the generated microwave waveform. However, the use of the ODL-based delay line allows the generation of an LCMW with a temporal duration that is  $N$  times as long as that of a microwave waveform generated by a one-time use of an LCFBG. The TBWP, on the other hand, can be controlled to be large by designing an FPI with two LCFBGs having wide bandwidths.

LCMW generation using the setup shown in Fig. 14(b) to generate two microwave waveforms was experimentally demonstrated. In a first demonstration, an FPI consisting of two LCFBGs with dispersion coefficients of  $\pm 19.6$  ps/nm with a physical spacing of 2 mm between the two LCFBGs was used as the spectral shaper. Fig. 15 shows two waveforms generated by the microwave waveform generator, by letting

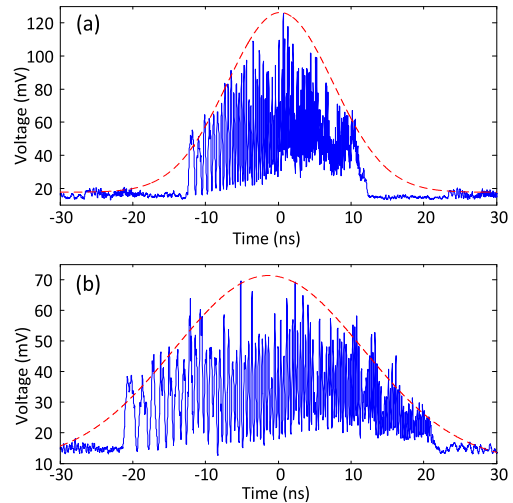


Fig. 15. Generated LCMWs using an FPI consisting of two LCFBGs with dispersion coefficients of  $\pm 19.6$  ps/nm with a physical spacing between the two LCFBGs of 2 mm with (a) three and (b) five round trips [50].

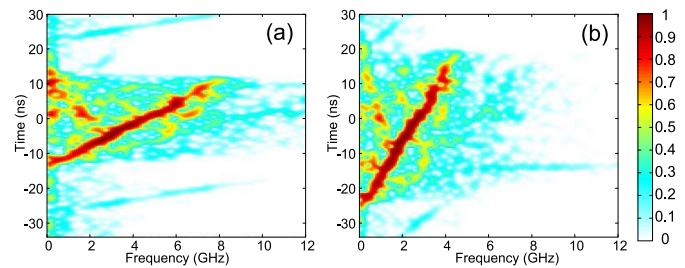


Fig. 16. Spectrograms of the LCMWs for (a) three and (b) five round trips. The color scale represents the normalized amplitude of the spectrogram [50].

the optical pulse recirculate in the ODL for three and five round trips. Extended temporal durations of around 25 and 42 ns were obtained for the two LCMWs, which exceed the 10 ns limit determined by the physical length of the LCFBG.

The spectrograms of the generated LCMWs are shown in Fig. 16. Linearly increasing instantaneous frequencies can be observed for the two generated LCMWs, which indicate a good linearity of the frequency chirping of the waveforms. The two LCMWs have bandwidths of 8.4 and 5.0 GHz with an identical TBWP of around 210. Since WTT mapping is only performed to part of the spectrum of the spectrally shaped pulse, due to the mismatch between the reflection bandwidths of the three LCFBGs, the temporal durations and bandwidths of the generated LCMWs are reduced, making the experimental TBWP smaller than the theoretical value of 310.

The central frequency of a generated LCMW can be changed using an FPI with a different cavity length. In a second demonstration, a second FPI consisting of two LCFBGs with the same dispersion coefficients of  $\pm 19.6$  ps/nm but with an increased physical spacing of  $d = 2$  cm was employed as the optical spectral shaper. The same ODL was used to perform WTT mapping. The LCMW for five round trips is shown in Fig. 17(a). A 45 ns long LCMW was generated. The minimum frequency is 1.5 GHz, instead of around DC for the LCMW shown in Fig. 15. A strong attenuation can

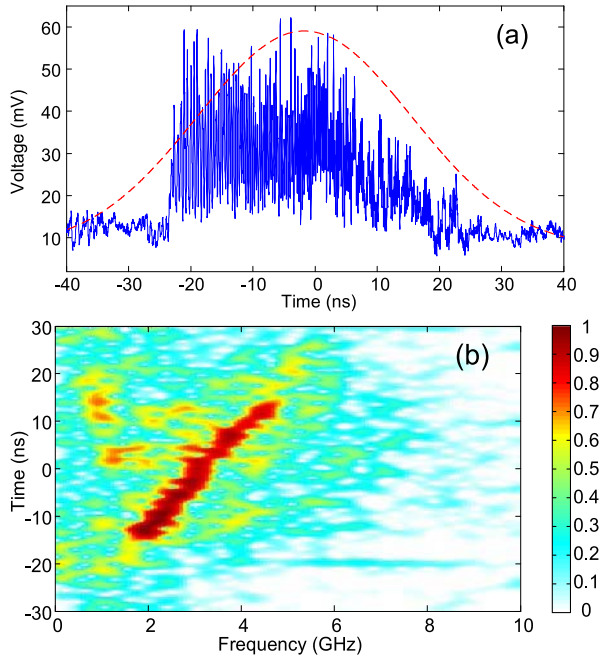


Fig. 17. (a) Generated LCMW using an FPI with an increased physical spacing of 2 cm for five round trips and (b) corresponding spectrogram. The color scale represents the normalized amplitude of the spectrogram [50].

be observed for the high frequency components due to a lower responsivity of the PD at a higher frequency band. The spectrogram in Fig. 17(b) indicates a good linearity of the frequency chirping of the waveform. The TBWP was calculated to be 180, which is smaller compared to that of the waveform generated using the FPI with a cavity of 2 mm. This is due to the lower responsivity of the PD at the higher frequency band, which makes the bandwidth of the generated LCMW smaller.

Amplitude ripples of the generated LCMWs can be observed in Figs. 15 and 17. The ripples are caused due to the lasing in the ODL since the gains at certain wavelengths are near the lasing threshold. To reduce or eliminate the ripples, a gain-flattening optical filter may be used to flatten the gain spectrum of the EDFA in the ODL so that the lasing can be suppressed.

Thanks to the use of the ODL, the waveforms shown in Figs. 15 and 17 have temporal durations as large as 42 ns, which are the longest temporal duration ever reported based on the SS-WTT mapping technique. For example, the generated LCMWs have temporal durations of 1 ns in [70] and [71], and 16 ns in [72]. An LCMW with a long temporal duration is important for long-range radar applications where a high average power is needed for long-range detection.

### C. True-Time Delay Beamforming

To achieve phased array beamforming, progressive phase or time delays are needed, which can be generated using phase shifters or true-time delay lines. In the past few years, numerous photonic true-time delay beamforming networks have been proposed. The key advantage of using true time delay lines for beamforming is the large instantaneous bandwidth, which is

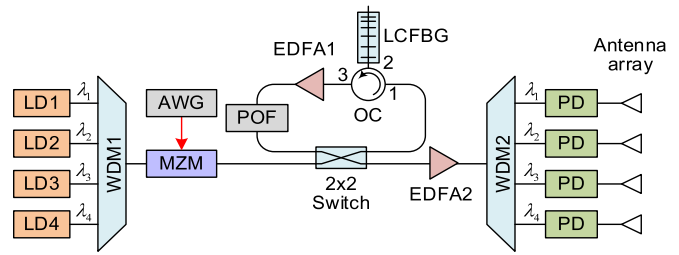


Fig. 18. Schematic of a true-time delay beamforming network using an ODL incorporating an LCFBG [51].

highly needed for broadband communications and radar applications [73]–[75]. True time delay lines may be implemented using electrical delay lines such as a SAW device [2]–[7], an EBG element [8]–[10], and an IC device that can be configured to let a microwave signal travel through different paths [11]–[13]. The major limitations of using electrical delay lines are the small operation bandwidth and small time delays. True time delay lines-based photonics can provide a much wider bandwidth and larger time delays. However, most of the beamforming networks based on photonic true-time delays require the use of a tunable laser source (TLS) array to achieve tunable time delays, which makes the system complicated and expensive. In addition, the wavelengths of the TLSs must be precisely tuned to ensure accurate tunable time delays. Due to the tuning nature of the wavelengths, the time delay accuracy is poorer than using fixed wavelengths. To achieve tunable time delays but with fixed wavelengths, a solution is to use a switch-controlled ODL incorporating an LCFBG [51].

The schematic of a four channel true-time delay beamforming network using a switch-controlled ODL incorporating an LCFBG is shown in Fig. 18 [51]. The light waves from four laser diodes (LDs) with four different wavelengths of  $\lambda_1$  to  $\lambda_4$  are combined at a wavelength-division multiplexer (WDM1) and sent to an MZM, where a microwave feed signal, generated by an electrical AWG, is modulated on the four wavelengths. The microwave-modulated optical signals at the output of the MZM are then launched into a switch-controlled ODL through a  $2 \times 2$  optical switch. An LCFBG is incorporated in the ODL via an OC to provide a wavelength-dependent time delay. An EDFA (EDFA1) is also incorporated in the ODL to compensate for the loss in the loop so that an optical signal can recirculate in the ODL for multiple round trips. A POF with four passbands centered at  $\lambda_1$  to  $\lambda_4$  is also employed to suppress the amplified spontaneous emission noise from EDFA1. The number of round trips is controlled by the  $2 \times 2$  optical switch. Note that the  $2 \times 2$  optical switch should be able to operate at a high speed to change its state within a time window when no signal is traveling through it, such a high-speed optical switch can be implemented, for example, based on an AlGaAs-GaAs platform, as reported in [76]. At the output of the loop, a second EDFA (EDFA2) is used to further amplify the optical signal and a second WDM (WDM2) is used to demultiplex the time-delayed optical signals, and sent to four PDs. The time delayed microwave signals are radiated to the free space via the array elements in a phased array antenna.

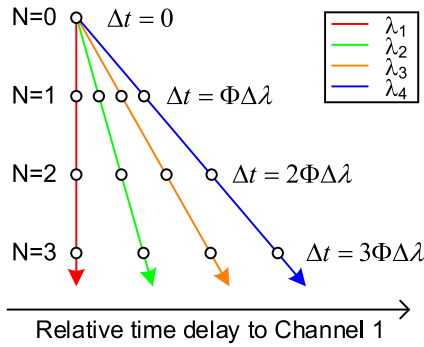


Fig. 19. Time delays of a signal in each channel relative to channel 1 as the number of round trips  $N$  increases [51].

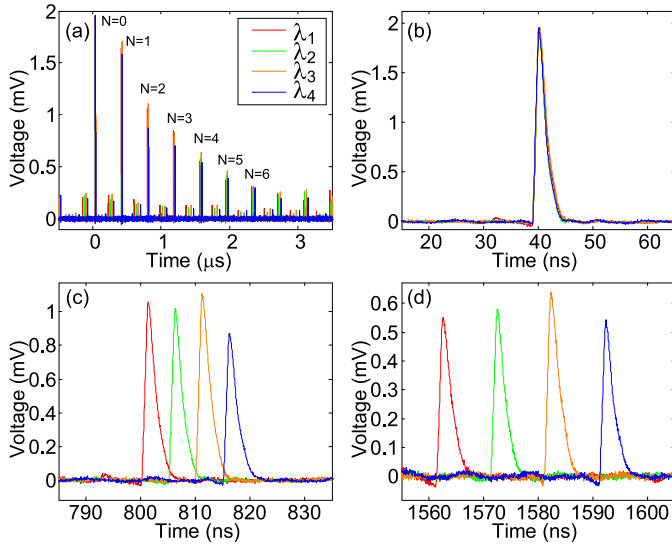


Fig. 20. Measured electrical signals at the outputs of the four PDs when an electrical pulse is applied to the MZM [51]. (a) Generated time delayed replicas and zoomed-in views for (b)  $N = 0$ , (c)  $N = 2$ , and (d)  $N = 4$ .

Due to the equivalent dispersion coefficient of  $N\Phi$  of the dispersive loop, where  $\Phi$  is the dispersion coefficient of the LCFBG in the loop, the time delay difference of a signal carried by two carrier wavelengths of  $\lambda_m$  and  $\lambda_n$  is given by

$$\Delta t = N\Phi(\lambda_n - \lambda_m) \quad (9)$$

It can be seen that progressive true-time delays can be obtained for the optical signals as the number of round trips  $N$  increases. The relationship between the time delays, the number of round trips and the carrier wavelengths are shown in Fig. 19. By increasing the number of round trips, a time-delay increment of  $\Phi\Delta\lambda$  can be achieved.

The generation of progressive time delays using the system shown in Fig. 18 was demonstrated. An electrical pulse with a temporal width of 1 ns is generated by an electrical AWG and applied to the MZM via the RF port, to modulate the four wavelengths at the MZM. The four wavelengths have a uniform wavelength spacing of 1 nm and are generated by the four LDs. The LCFBG in the ODL has a dispersion coefficient of 2500 ps/nm. The time delayed waveforms detected at the outputs of the four PDs are shown in Fig. 20(a).

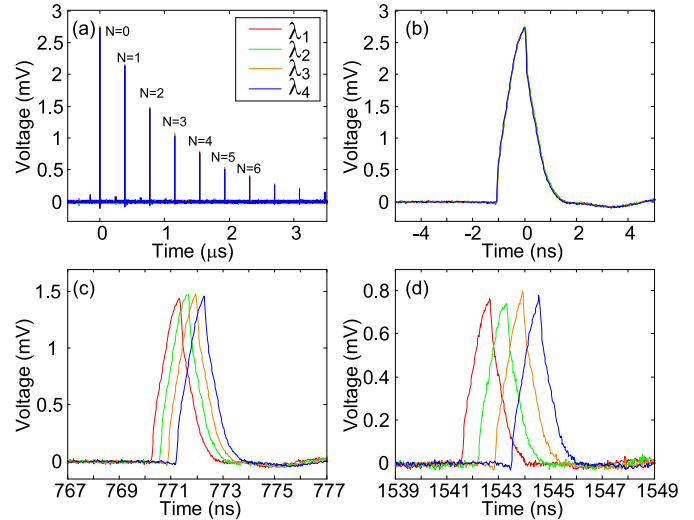


Fig. 21. Measured electrical signals at the outputs of the four PDs with a small true-time delay step of 160 ps [51]. (a) Generated time delayed replicas and zoomed-in view of the signals for (b)  $N = 0$ , (c)  $N = 2$ , and (d)  $N = 4$ .

Multiple time-delayed replicas of the electrical pulse are detected at the output of each channel with a repetition time of around 380 ns, which is the round trip time of an optical pulse traveling in the ODL. In addition, the pulses from the four channels overlap in time only for  $N = 0$  and an increasing time delay difference between two adjacent time-delayed pulses can be observed for  $N > 0$ , indicating that progressive true-time delays are generated when the optical pulses start to recirculate in the ODL. Note that the amplitudes of the time-delayed pulses are decaying as  $N$  increases. This is again caused by a slightly less than 1 net gain of the loop, which is intentionally set to avoid possible lasing. Nevertheless, the pulses can still recirculate for more than 10 round trips before being immersed in noise. The reduced amplitudes may be compensated by a microwave power amplifier that is commonly used in a phase array antenna.

Detected waveforms with more details are shown in Fig. 20(b)–(d) for different numbers of round trips of 0, 2, and 4. The time spacing between two pulses from two adjacent channels are measured to be 5.0 and 10.0 ns for  $N = 2$  and  $N = 4$ . The progressive time delays are as predicted in Fig. 19, and are in perfect agreement with the theoretical values of 2.5 ns per round trip. Assuming that the true-time delayed waveforms are sent to a phased array antenna with a uniform element spacing of 5 m, a steering angle of  $8.6^\circ$  per round trip can be achieved. If the signal can recirculate in the loop for 12 round trips, the scanning range can be from  $-60^\circ$  to  $60^\circ$ .

In a high-resolution radar, the element spacing may be smaller, a smaller true-time delay increment may be needed. For such applications, the true-time delays per round trip can be changed using an LCFBG with a smaller dispersion coefficient or an LD array with a smaller wavelength spacing. Here, an LCFBG with a smaller dispersion coefficient of 200 ps/nm is employed, and the wavelength spacing of the laser array is set at a fixed value of 0.8 nm. Fig. 21 shows the

measured time-delayed signals when a 1 ns electrical pulse is modulated on the multiwavelength carriers. The measured true-time delay difference is 159.2 ps per round trip. Assuming that the element spacing is 0.2 m, the true-time delay corresponds to a steering angle of 13.9°.

It should be noted that, the true-time delay beamforming system is suitable for applications where the transmitted signal is pulsed. In addition, the beam steering speed is determined by both the round trip time of the loop and the maximum number of round trips that the signal recirculates in the loop to achieve the required time delay. Assuming that a microwave signal is required to recirculate for 10 round trips, the time interval between adjacent beam steering angles is 3.8  $\mu$ s, which is still very fast and sufficient for most applications.

#### IV. CONCLUSION

An overview on our recent work using a photonic DDL for broadband microwave signal processing was presented. By using an FBG-based photonic DDL, microwave time reversal and temporal convolution were demonstrated. To have a DDL with a larger dispersion, an ODL incorporating an LCFBG was proposed. The ODL was used for the implementation of microwave time-stretched sampling, microwave generation with an extended temporal duration and wideband true-time delay beamforming.

The key advantage of using photonics to process microwave signals is the wide bandwidth. The microwave photonic signal processors discussed in this paper can have a bandwidth from tens of GHz to a few THz. Currently, although commercially available electronic signal processors can process a signal with a bandwidth of tens of GHz, photonics-assisted signal processing may still be the only solution when a very large operation bandwidth is required, for example, from hundreds of GHz up to THz range.

The microwave photonic signal processors discussed in this paper were implemented based on fiber optics, which are bulky and sensitive to environmental interferences. Thanks to the recent development of the photonic ICs (PICs) [77], realizing such signal processors using PICs has become possible. For example, a linearly chirped waveguide grating has been fabricated on a silicon-on-insulator platform to provide a dispersion coefficient of 20.7 ps/nm [78]. A 27 m long silicon waveguide has been demonstrated with a low loss of 0.08 dB/m [79]. Such components can be readily used to develop on-chip chirped-grating-based DDLs and dispersive loops, which are the key components for the implementation of the microwave photonic signal processors discussed in this paper.

#### REFERENCES

- [1] H. Shahoei and J. P. Yao, "Delay lines," in *Wiley Encyclopedia of Electrical and Electronics Engineering*, New York, NY, USA: Wiley, Dec. 2014, pp. 1–15, doi: 10.1002/047134608X.W8234.
- [2] R. Weigel *et al.*, "Microwave acoustic materials, devices, and applications," *IEEE Trans. Microw. Theory Techn.*, vol. 50, no. 3, pp. 738–749, Mar. 2002.
- [3] F. Zheng and T. Kaiser, *Digital Signal Processing for RFID*. Hoboken, NJ, USA: Wiley, 2016.
- [4] C. C. W. Ruppel, C. Kappacher, L. Reindl, and G. Visitini, "Design and compensation of nonequidistantly sampled SAW transducers," in *Proc. IEEE Ultrason. Symp.*, Sep. 1989, pp. 19–23.
- [5] L. Reindl, U. Rosler, C. C. W. Ruppel, R. Obertreis, and R. Weigel, "Chirped SAW devices for wireless passive sensors," in *Proc. IEEE Ultrason. Symp.*, Oct. 1997, pp. 343–347.
- [6] P. Santos *et al.*, "Gigahertz monolithic delay lines for surface acoustic waves on Silicon," *IOP Conf. Ser. Mater. Sci. Eng.*, vol. 41, no. 1, p. 012009, 2012.
- [7] S. Büyükköse, B. Vratzov, J. van der Veen, P. Santos, and W. van der Wiel, "Ultrahigh-frequency surface acoustic wave generation for acoustic charge transport in silicon," *Appl. Phys. Lett.*, vol. 102, p. 013112, Jan. 2013.
- [8] G. Keiser, *Optical Fiber Communications*. Hoboken, NJ, USA: Wiley, 2003.
- [9] M. A. G. Laso *et al.*, "Chirped delay lines in microstrip technology," *IEEE Microw. Wireless Compon. Lett.*, vol. 11, no. 12, pp. 486–488, Dec. 2001.
- [10] J. D. Schwartz, Q. Zhuge, J. Azaña, and D. V. Plant, "1-D uniform and chirped electromagnetic bandgap structures in substrate integrated waveguides at 60 GHz," *Microw. Opt. Technol. Lett.*, vol. 54, no. 3, pp. 735–737, Mar. 2012.
- [11] F. Sangster, "Integrated MOS and bipolar analog delay lines using bucket-brigade capacitor storage," in *IEEE Int. Solid-State Circuits Conf. Dig. Tech. Papers.*, Sep. 1970, pp. 74–75.
- [12] J. Roderick, H. Krishnaswamy, K. Newton, and H. Hashemi, "Silicon-based ultra-wideband beam-forming," *IEEE J. Solid-State Circuits*, vol. 41, no. 8, pp. 1726–1739, Aug. 2006.
- [13] T.-S. Chu, J. Roderick, and H. Hashemi, "An integrated ultra-wideband timed array receiver in 0.13  $\mu$ m CMOS using a path-sharing true time delay architecture," *IEEE J. Solid-State Circuits*, vol. 42, no. 12, pp. 2834–2850, Dec. 2007.
- [14] J. Polivka, "An overview of microwave sensor technology," *High Freq. Electron.*, vol. 6, pp. 32–42, Sep. 2007.
- [15] M. I. Skolnik, *RADAR Systems*. New York, NY, USA: McGraw-Hill, 2001.
- [16] J. Yao, "Microwave photonics," *J. Lightw. Technol.*, vol. 27, no. 3, pp. 314–335, Feb. 1, 2009.
- [17] J. Capmany and D. Novak, "Microwave photonics combines two worlds," *Nature Photon.*, vol. 1, no. 6, pp. 319–330, Apr. 2007.
- [18] T. Erdogan, "Fiber grating spectra," *J. Lightw. Technol.*, vol. 15, no. 8, pp. 1277–1294, Aug. 1997.
- [19] S. Yegnanarayanan, P. D. Trinh, F. Coppinger, and B. Jalali, "Compact silicon-based integrated optic time delays," *IEEE Photon. Technol. Lett.*, vol. 9, no. 5, pp. 634–635, May 1997.
- [20] J. Cardenas *et al.*, "Wide-bandwidth continuously tunable optical delay line using silicon microring resonators," *Opt. Exp.*, vol. 18, no. 25, pp. 26525–26534, Dec. 2010.
- [21] M. S. Rasras *et al.*, "Integrated resonance-enhanced variable optical delay lines," *IEEE Photon. Technol. Lett.*, vol. 17, no. 4, pp. 834–836, Apr. 2005.
- [22] J. Mack, E. Burmeister, H. Poulsen, B. Stamenic, J. Bowers, and D. Blumenthal, "Photonic integrated circuit switch matrix and waveguide delay lines for optical packet synchronization," in *Proc. 34th Eur. Conf. Opt. Commun.*, Sep. 2008, pp. 1–2.
- [23] T. Baba, "Slow light in photonic crystals," *Nature Photon.*, vol. 2, no. 8, pp. 465–473, 2008.
- [24] Y. Hamachi, S. Kubo, and T. Baba, "Slow light with low dispersion and nonlinear enhancement in a lattice-shifted photonic crystal waveguide," *Opt. Lett.*, vol. 34, no. 7, pp. 1072–1074, Apr. 2009.
- [25] Y. Dai and J. P. Yao, "Nonuniformly spaced photonic microwave delay-line filters and applications," *IEEE Trans. Microw. Theory Techn.*, vol. 58, no. 11, pp. 3279–3289, Nov. 2010.
- [26] J. Mora *et al.*, "Photonic microwave tunable single-bandpass filter based on a Mach-Zehnder interferometer," *J. Lightw. Technol.*, vol. 24, no. 7, pp. 2500–2509, Jul. 2006.
- [27] X. Xue, X. Zheng, H. Zhang, and B. Zhou, "High-Q single-bandpass photonic RF filter overcoming optical third-order dispersion based on programmable spectrum shaping of a broadband optical source," presented at the OFC, 2013.
- [28] T. Jansson, "Real-time Fourier transformation in dispersive optical fibers," *Opt. Lett.*, vol. 8, no. 4, pp. 232–234, Apr. 1983.
- [29] M. A. Muriel, J. Azaña, and A. Carballar, "Real-time Fourier transformer based on fiber gratings," *Opt. Lett.*, vol. 24, no. 1, pp. 1–3, Jan. 1999.
- [30] M. Li, Y. Han, S. Pan, and J. P. Yao, "Experimental demonstration of symmetrical waveform generation based on amplitude-only modulation in a fiber-based temporal pulse shaping system," *IEEE Photon. Technol. Lett.*, vol. 23, no. 11, pp. 715–717, Jun. 1, 2011.

- [31] C. Wang and J. Yao, "Chirped microwave pulse compression using a photonic microwave filter with a nonlinear phase response," *IEEE Trans. Microw. Theory Techn.*, vol. 57, no. 2, pp. 496–504, Feb. 2009.
- [32] Y. Dai and J. P. Yao, "Microwave correlator based on a nonuniformly spaced photonic microwave delay-line filter," *IEEE Photon. Technol. Lett.*, vol. 21, no. 14, pp. 969–971, Jul. 15, 2009.
- [33] C. Wang, M. Li, and J. P. Yao, "Continuously tunable photonic microwave frequency multiplication by use of an unbalanced temporal pulse shaping system," *IEEE Photon. Technol. Lett.*, vol. 22, no. 17, pp. 1285–1287, Sep. 1, 2010.
- [34] H. Shahoei and J. P. Yao, "Continuously tunable microwave frequency multiplication by optically pumping linearly chirped fiber Bragg gratings in an unbalanced temporal pulse shaping system," *J. Lightw. Technol.*, vol. 30, no. 12, pp. 1954–1959, Jun. 15, 2012.
- [35] F. Coppinger, A. S. Bhushan, and B. Jalali, "Photonic time stretch and its application to analog-to-digital conversion," *IEEE Trans. Microw. Theory Techn.*, vol. 47, no. 7, pp. 1309–1314, Jul. 1999.
- [36] F. Coppinger, A. S. Bhushan, and B. Jalali, "Time magnification of electrical signals using chirped optical pulses," *Electron. Lett.*, vol. 34, no. 4, pp. 399–400, Feb. 1998.
- [37] H. Chi, Y. Chen, Y. Mei, X. Jin, S. Zheng, and X. Zhang, "Microwave spectrum sensing based on photonic time stretch and compressive sampling," *Opt. Lett.*, vol. 38, no. 2, pp. 136–138, Jan. 2013.
- [38] Y. Chen, H. Chi, T. Jin, S. Zheng, X. Jin, and X. Zhang, "Sub-Nyquist sampled analog-to-digital conversion based on photonic time stretch and compressive sensing with optical random mixing," *J. Lightw. Technol.*, vol. 31, no. 21, pp. 3395–3401, Nov. 1, 2013.
- [39] B. W. Buckley, A. M. Madni, and B. Jalali, "Coherent time-stretch transformation for real-time capture of wideband signals," *Opt. Exp.*, vol. 21, no. 8, pp. 21618–21627, Sep. 2013.
- [40] Y. Han and B. Jalali, "Continuous-time time-stretched analog-to-digital converter array implemented using virtual time gating," *IEEE Trans. Circuits Syst. I, Reg. Papers*, vol. 52, no. 8, pp. 1502–1507, Aug. 2005.
- [41] M. H. Asghari and B. Jalali, "Anamorphic transformation and its application to time-bandwidth compression," *Appl. Opt.*, vol. 52, no. 27, pp. 6735–6743, Sep. 2013.
- [42] M. H. Asghari and B. Jalali, "Experimental demonstration of optical real-time data compression," *Appl. Phys. Lett.*, vol. 104, p. 111101, Mar. 2014.
- [43] J. Chou, O. Boyraz, D. Solli, and B. Jalali, "Femtosecond real-time single-shot digitizer," *Appl. Phys. Lett.*, vol. 91, no. 16, p. 161105, Oct. 2007.
- [44] B. M. Jung and J. Yao, "A two-dimensional optical true time-delay beamformer consisting of a fiber Bragg grating prism and switch-based fiber-optic delay lines," *IEEE Photon. Technol. Lett.*, vol. 21, no. 10, pp. 627–629, May 15, 2009.
- [45] S. Blais and J. Yao, "Photonic true-time delay beamforming based on superstructured fiber Bragg gratings with linearly increasing equivalent chirps," *J. Lightw. Technol.*, vol. 27, no. 9, pp. 1147–1154, May 1, 2009.
- [46] J. Zhang and J. P. Yao, "Broadband and precise microwave time reversal using a single linearly chirped fiber Bragg grating," in *Proc. 9th Asia-Pacific Microw. Photon. Conf. Int. Topical Meeting Microw. Photon.*, Oct. 2014, pp. 57–60, paper TuD-2.
- [47] J. Zhang and J. P. Yao, "Broadband and precise microwave time reversal using a single linearly chirped fiber Bragg grating," *IEEE Trans. Microw. Theory Techn.*, vol. 63, no. 7, pp. 2166–2172, Jul. 2015.
- [48] J. Zhang and J. P. Yao, "Photonic-assisted microwave temporal convolution," *J. Lightw. Technol.*, vol. 34, no. 20, p. 4652, Sep. 1, 2016.
- [49] J. Zhang and J. Yao, "Time-stretched sampling of a fast microwave waveform based on the repetitive use of a linearly chirped fiber Bragg grating in a dispersive loop," *Optica*, vol. 1, no. 2, pp. 64–69, Aug. 2014.
- [50] J. Zhang, O. L. Coutinho, and J. P. Yao, "A photonic approach to linearly chirped microwave waveform generation with an extended temporal duration," *IEEE Trans. Microw. Theory Techn.*, vol. 64, no. 6, pp. 1947–1953, Jun. 2016.
- [51] J. Zhang and J. P. Yao, "Photonic true-time delay beamforming using a switch-controlled wavelength-dependent recirculating loop," *J. Lightw. Technol.*, vol. 34, no. 16, pp. 3923–3929, Aug. 12, 2016.
- [52] E. H. Zhou, H. Ruan, C. Yang, and B. Judkewitz, "Focusing on moving targets through scattering samples," *Optica*, vol. 1, no. 4, pp. 227–232, Oct. 2014.
- [53] G. Lerosey, J. De Rosny, A. Tourin, and M. Fink, "Focusing beyond the diffraction limit with far-field time reversal," *Science*, vol. 315, no. 5815, pp. 1120–1122, Feb. 2007.
- [54] G. Lerosey, J. De Rosny, A. Tourin, A. Derode, G. Montaldo, and M. Fink, "Time reversal of electromagnetic waves," *Phys. Rev. Lett.*, vol. 92, no. 19, p. 193904, May 2004.
- [55] G. Lerosey, J. De Rosny, A. Tourin, A. Derode, and M. Fink, "Time reversal of wideband microwaves," *Appl. Phys. Lett.*, vol. 88, no. 15, Apr. 2006, Art. no. 154101.
- [56] A. Dezfouliyan and A. M. Weiner, "Experimental investigation of UWB impulse response and time reversal technique up to 12 GHz: Omnidirectional and directional antennas," *IEEE Trans. Antennas Propag.*, vol. 60, no. 7, pp. 3407–3415, Jul. 2012.
- [57] J. de Rosny, G. Lerosey, and M. Fink, "Theory of electromagnetic time-reversal mirrors," *IEEE Trans. Antennas Propag.*, vol. 58, no. 10, pp. 3139–3149, Oct. 2010.
- [58] P. Kosmas and C. M. Rappaport, "Time reversal with the FDTD method for microwave breast cancer detection," *IEEE Trans. Microw. Theory Techn.*, vol. 53, no. 7, pp. 2317–2323, Jul. 2005.
- [59] P. Kosmas and C. M. Rappaport, "FDTD-based time reversal for microwave breast cancer detection-localization in three dimensions," *IEEE Trans. Microw. Theory Techn.*, vol. 54, no. 4, pp. 1921–1927, Jun. 2006.
- [60] B. Guo, L. Xu, and J. Li, "Time reversal based microwave hyperthermia treatment of breast cancer," in *Proc. 39th Asilomar Conf. Signals, Syst. Comput. Conf. Rec.*, Oct. 2005, pp. 290–293.
- [61] H. D. Trefná, J. Vrba, and M. Persson, "Time-reversal focusing in microwave hyperthermia for deep-seated tumors," *Phys. Med. Biol.*, vol. 55, no. 8, pp. 2167–2185, Mar. 2010.
- [62] P. Kosmas, E. Zastrow, S. C. Hagness, and B. D. V. Veen, "A computational study of time reversal techniques for ultra-wideband microwave hyperthermia treatment of breast cancer," in *Proc. IEEE/SP 14th Workshop Statist. Signal Process. (SSP)*, Aug. 2007, pp. 312–316.
- [63] A. E. Campbell-Washburn, H. Xue, R. J. Lederman, A. Z. Faranesh, and M. S. Hansen, "Real-time distortion correction of spiral and echo planar images using the gradient system impulse response function," *Magn. Reson. Med.*, vol. 75, no. 6, pp. 2278–2285, Jun. 2015, doi: 10.1002/mrm.25788.
- [64] M. E. I. Martínez and F. E. H. Montero, "Detection of periodic signals in noise based on higher-order statistics joined to convolution process and spectral analysis," in *Progress in Pattern Recognition, Image Analysis, Computer Vision, and Applications*. Berlin, Germany: Springer, 2013, pp. 488–495.
- [65] J. Yao, "Photonic generation of microwave arbitrary waveforms," *Opt. Commun.*, vol. 284, no. 15, pp. 3723–3736, Jul. 2011.
- [66] D. K. Barton, *Radar System Analysis and Modeling*. Norwood, MA, USA: Artech House, 2004.
- [67] A. W. Rihaczek, *Principles of High-Resolution Radar*. New York, NY, USA: McGraw-Hill, 1969.
- [68] R. Skaug and J. F. Hjelmsstad, *Spread Spectrum in Communication*. London, U.K.: Peregrinus, 1985.
- [69] M. Bertero, M. Miyakawa, P. Boccacci, F. Conte, K. Orikasa, and M. Furutani, "Image restoration in chirp-pulse microwave CT (CP-MCT)," *IEEE Trans. Biomed. Eng.*, vol. 47, no. 5, pp. 690–699, May 2000.
- [70] H. Shahoei and J. P. Yao, "Continuously tunable chirped microwave waveform generation using a tilted fiber Bragg grating written in an erbium/ytterbium co-doped fiber," *IEEE Photon. J.*, vol. 4, no. 3, pp. 765–771, Jun. 2012.
- [71] M. H. Khan *et al.*, "Ultrabroad-bandwidth arbitrary radiofrequency waveform generation with a silicon photonic chip-based spectral shaper," *Nature Photon.*, vol. 4, no. 2, pp. 117–122, Feb. 2010.
- [72] A. Rashidinejad and A. M. Weiner, "Photonic radio-frequency arbitrary waveform generation with maximal time-bandwidth product capability," *J. Lightw. Technol.*, vol. 32, no. 20, pp. 3383–3393, Oct. 15, 2014.
- [73] Y. Liu, J. P. Yao, and J. Yang, "Wideband true-time-delay unit for phased array beamforming using discrete-chirped fiber grating prism," *Opt. Commun.*, vol. 207, no. 1, pp. 177–187, Jun. 2002.
- [74] D.-H. Yang and W.-P. Lin, "Phased-array beam steering using optical true time delay technique," *Opt. Commun.*, vol. 350, pp. 90–96, Sep. 2015.
- [75] X. Ye, F. Zhang, and S. Pan, "Optical true time delay unit for multi-beamforming," *Opt. Exp.*, vol. 23, no. 8, pp. 10002–10008, Apr. 2015.
- [76] Q. Wang and J. P. Yao, "A high speed 2×2 electro-optic switch using a polarization modulator," *Opt. Exp.*, vol. 15, no. 25, pp. 16500–16505, Dec. 2007.
- [77] W. Zhang and J. P. Yao, "Silicon-based integrated microwave photonics," *IEEE J. Quantum Electron.*, vol. 52, no. 1, Jan. 2016, Art. no. 0600412.

- [78] W. Zhang and J. P. Yao, "Photonic generation of linearly chirped microwave waveforms using a silicon-based on-chip spectral shaper incorporating two linearly chirped waveguide Bragg gratings," *J. Lightw. Technol.*, vol. 33, no. 24, pp. 5047–5054, Dec. 12, 2015.
- [79] H. Lee, T. Chen, J. Li, O. Painter, and K. J. Vahala, "Ultra-low-loss optical delay line on a silicon chip," *Nat. Commun.*, vol. 3, p. 867, May 2012.

**Jiejun Zhang** (S'12) received the B.Eng. degree in electronic science and technology from the Harbin Institute of Technology, Harbin, China, in 2010, and the M.Sc. degree in optical engineering from the Huazhong University of Science and Technology, Wuhan, China. He is currently pursuing the Ph.D. degree in electrical engineering at the Microwave Photonics Research Laboratory, School of Electrical Engineering and Computer Science, University of Ottawa, Ottawa, ON, Canada.

His current research interests include photonic generation of microwave waveforms, photonic processing of microwave signals, and fiber optic sensors.

**Jianping Yao** (M'99–SM'01–F'12) received the Ph.D. degree in electrical engineering from the Université de Toulon et du Var, Le Garde, France, in 1997.

From 1998 to 2001, he was with the School of Electrical and Electronic Engineering, Nanyang Technological University, Singapore, as an Assistant Professor. In 2001, he joined the School of Electrical Engineering and Computer Science, University of Ottawa, Ottawa, ON, Canada, as an Assistant Professor, where he became an Associate Professor in 2003, and a Full Professor in 2006. He was appointed the University Research Chair in Microwave Photonics in 2007. In 2016, he was conferred the title of Distinguished University Professor of the University of Ottawa. From 2007 to 2010 and from 2013 to 2016, he was the Director of the Ottawa–Carleton Institute for Electrical and Computer Engineering. He is currently a Professor and the University Research Chair with the School of Electrical Engineering and Computer Science, University of Ottawa. He has authored or co-authored more than 520 research papers, including more than 310 papers in peer-reviewed journals and 210 papers in conference proceedings.

Prof. Yao is a Registered Professional Engineer in the Province of Ontario. He is a Fellow of the Optical Society of America and the Canadian Academy of Engineering. He was an IEEE MTT-S Distinguished Microwave Lecturer for 2013–2015. He is a Topical Editor of *Optics Letters*, and serves on the Editorial Boards of the IEEE TRANSACTIONS ON MICROWAVE THEORY AND TECHNIQUES, *Optics Communications*, *Frontiers of Optoelectronics*, and *Science Bulletin*. He was as a Guest Co-Editor of a Focus Issue on Microwave Photonics in *Optics Express* in 2013 and a Lead-Editor of a Feature Issue on Microwave Photonics in *Photonics Research* in 2014. He is a Chair of numerous international conferences, symposia, and workshops, including the Vice Technical Program Committee (TPC) Chair of the IEEE Microwave Photonics Conference in 2007, a TPC Co-Chair of the Asia–Pacific Microwave Photonics Conference in 2009 and 2010, a TPC Chair of the high-speed and broadband wireless technologies subcommittee of the IEEE Radio Wireless Symposium in 2009–2012, a TPC Chair of the microwave photonics subcommittee of the IEEE Photonics Society Annual Meeting in 2009, a TPC Chair of the IEEE Microwave Photonics Conference in 2010, a General Co-Chair of the IEEE Microwave Photonics Conference in 2011, a TPC Co-Chair of the IEEE Microwave Photonics Conference in 2014, and a General Co-Chair of the IEEE Microwave Photonics Conference in 2015. He is also a Committee member of numerous international conferences, such as IPC, OFC, BGPP, and MWP. He was a recipient of the 2005 International Creative Research Award of the University of Ottawa. He was a recipient of the 2007 George S. Glinski Award for Excellence in Research. In 2008, he was the recipient of the Natural Sciences and Engineering Research Council of Canada Discovery Accelerator Supplements Award. He was also the recipient of an inaugural OSA Outstanding Reviewer Award in 2012.